2. Methods

2.1 Bubble liposomes

We used Bubble liposomes prepared with polyethyleneglycol-modified liposomes (PEG-liposomes) and perfluoropropane gas (Takachiho Chemical Inc., Co., Ltd., Tokyo, Japan). The liposomes were prepared by a reverse-phase evaporation method, as described previously[10]. To prepare liposomes for the BLs, 1, 2-distearoyl-sn-glycero-phosphatidylcholine (DSPC) and 1, 2-distearoyl-sn-glycero-3-phosphatidyl-ethanolamine-methoxypolyethyleneglycol [DSPE-PEG (2k) -OMe] were mixed at a molar ratio of 94:6. First, 5 mL sterilized vials containing 2 mL of PEG-liposome suspension (lipid concentration: 1 mg/mL) were placed in vials supercharged with 7.5 mL of perfluoropropane (C_3F_8) gas, then sonicated by continuous ultrasound at a frequency of 42 kHz for two or three min. During this process, gas was trapped inside the liposomes, resulting in a cloudy suspension. A bath-type ultrasound cleaner (Branson 2510) was used for sonication. **Figure 1** shows an image of BLs under a microscope equipped with a Darklite Illuminator (NEPA Gene Co. Ltd., Chiba, Japan). **Figure 2** shows the size distribution of BLs and Sonazoid measured by dynamic light scattering (ELS-Z, Otsuka Electronics Co., Ltd., Osaka, Japan). Although sub-micron sized objects are not shown in the microscopic image, **Fig. 2** indicates that the average diameters of BLs are approximately 400 to 500 nm and are smaller than the conventional MBs Sonazoid. **Table 1** shows the characteristics of BLs and another type of MBs F-04E[6, 7]. The suspension of BLs was freshly prepared before the experiment, diluted with saline to a concentration of 0.01–0.05 mg lipid/ml.

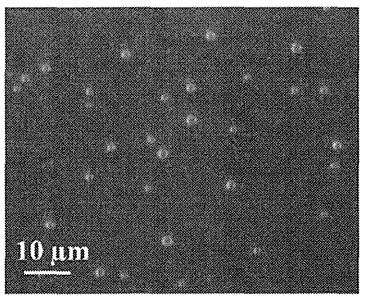

Fig. 1 Microscopic image of BLs.

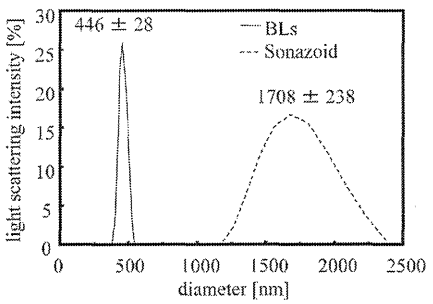

Fig. 2 Size distribution of BLs and Sonazoid.

2.2 Experimental setup

We prepared an artificial blood vessel with a Y-form bifurcation structure, which was made of a mixture of wax and poly (vinyl alcohol) (PVA) [11]. The inflow path of 2 mm was repeatedly divided into two lower courses to provide artificial capillaries until the middle of the model, where the minimum path width was 0.50 mm. The path widths and the cross-sectional areas were designed to guarantee a constant flow velocity in any part of the model. The whole view, *x-y* plane view and *x-z* plane view of the experimental setup are shown in **Fig. 3a, b and c**, respectively. The artificial blood vessel with external dimensions of 180 × 70 × 8 mm^3, was positioned 30 mm above the bottom of a water tank, to prevent multiple reflections of ultrasound between the artificial blood vessel and the bottom of the tank. The blood vessel was divided into Paths A and B with a branch angle of 75 degrees. The path widths w_1 and w_2 corresponded to 1.4 mm and 1.0 mm, respectively. We used an optical microscope (Hirox KH-7700) to observe the area of interest in the blood vessel. The image size was 800 × 600 pixels and the optical resolution of the digitized images was 31.5 μm per pixel. The light source was located above

Table 1 Characteristics of BLs and MBs.

	BLs	*MBs (F-04E[6, 7])*
Mean diameter [μm]	0.4–0.5	2.7
Shell	Lipid (bilayer)	PVC-AN copolymer
Gas	C_3F_8	C_3H_8, C_4H_{10}

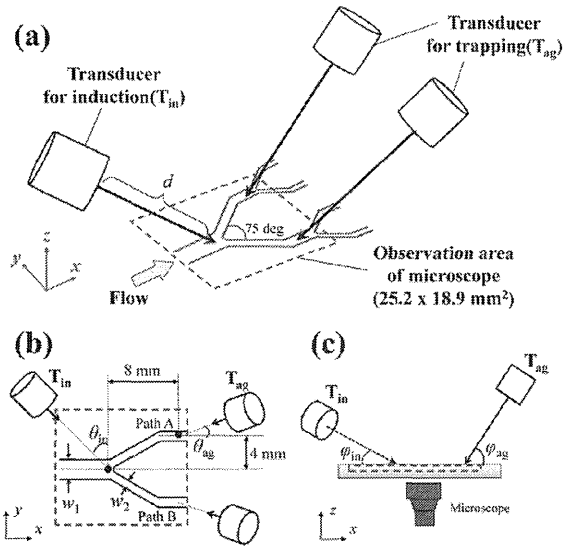

Fig. 3 Schematic presentation of the experiment with the artificial blood vessel, the microscope and the ultrasound transducers.

the water tank. We set transducer T_{in}, consisting of a concave ceramic disc, to emit focused ultrasound for induction. We prepared four different ultrasound transducers T_{in} to compare the effect of frequency. The central frequencies of the T_{in} were 3, 5, 7 and 10 MHz, and the apertures were 18, 15, 12 and 10 mm, respectively. The focal lengths of individual transducers ranged from 53 to 62 mm. Kudo *et al.* [12] reported stability of oscillating BLs under wideband ultrasound pulses at a central frequency of 10 MHz. We investigated frequencies below 10 MHz, considering the frequency range of clinical ultrasound. The focal position of T_{in} was fixed at the bifurcation point. The angle of the axis of T_{in} was set at $\theta_{in} = 45$ degree and $\varphi_{in} = 30$ degree. In our previous study [7], we investigated the controllability of MBs in a sound pressure range of 100 to 500 kPa-pp because of output bound of the elements of the transducers. In the present study, we set the sound pressures at 100, 200, 300, 400 and 500 kPa-pp.

Other transducers T_{ag} were newly introduced for evaluation of the controllability of BLs, as mentioned in the next section. The transducer T_{ag} was the same as one of the T_{in}, which consisted of a concave ceramic disc with a central frequency of 5 MHz and an aperture of 15 mm. The focal length of the T_{ag} was 58 mm. We set the axis of one T_{ag} to correspond to the center of the axis of the Path A. The focal point of T_{ag} was located 8 mm on the x-axis and 4 mm on the y-axis from the bifurcation point. The other T_{ag} was located in the middle of Path B (8 mm on the x-axis and 4 mm on the y-axis from the bifurcation point). We set the maximum sound pressure of T_{ag} at 500 kPa-pp. The angle of the axis of T_{ag} was set at $\theta_{ag} = 20$ degree and $\varphi_{ag} = 60$ degree. The distance of the transducers from the blood vessel was set at $d = 60$ mm. Sinusoidal waves with frequencies of 3, 5, 7 and 10 MHz were generated by an oscillator and applied to transducers T_{in} and T_{ag}. **Figure 4** shows an overview of the experimental setup.

2.3 Measurement of the area of trapped BLs

In our previous studies [6, 7, 11], we evaluated the controllability of MBs by defining the induction index that reflects the brightness according to the presence of bubbles in two paths (Path A and B). However, because of the size and low concentration of BLs, observation of brightness was difficult. Thus, we calculated the area of trapped BLs in each path and defined a new induction index as follows. To measure the number of BLs, we established three square regions of interest (ROI) in the path before bifurcating (ROI O) and in Paths A and B (ROIs A and B), respectively. **Figure 5** shows the configuration between transducers T_{ag} and the ROIs. The transducer drawn in dotted line (T_{ag}'), which was the same type of transducer as the other two T_{ag}, targeted a point 5 mm upstream from the bifurcation point. The angles of the axis of T_{ag}' were set at $(\theta_{ag}, \varphi_{ag}) = (0, 60)°$. This configuration was set to confirm the degree of conservation of the number of BLs before and after the bifurcation.

The width of each ROI corresponded to the path width, and the length of each ROI (L) was set by considering the ultrasound beam width. In our previous research [8, 9], the half-widths of ultrasound beams at 3 and 10 MHz were 1.7 and 1.1 mm, respectively. We set L and L_0 at 6.5 and 10.0 mm, which were much larger than the ultrasound beam width. Then, when the size of ROI A or B was 1.1×6.5 mm^2 and the size of ROI O was 1.6×10.0 mm^2, we calculated the area of trapped BLs. To evaluate the controllability of the amount of BLs quantitatively, image processing [8] was used to calculate the area of BL aggregates trapped by T_{ag} in the middle of the path. **Figure 6** shows the image processing procedure for measuring the areas of trapped BLs in ROIs A and B. The outline of the blood vessel was overlapped as the dotted lines in the images. The microscopic image was recorded continuously as a video file from the beginning of the experiment. Then the area of trapped BLs was extracted by subtracting the initial image from the images after aggregates of BLs were formed. Finally, the area of trapped BLs was obtained from the binary image by discriminant analysis method.

Figure 7 shows the changes over time of the areas of trapped BLs in ROIs A and B upon injection of the BL suspension with ultrasound emissions from both T_{in} and T_{ag}. The maximum sound pressure of T_{in} was 200 kPa-pp and the concentration of BLs suspension was 0.02 mg lipid/ml. Before injection, the trapped area remained at

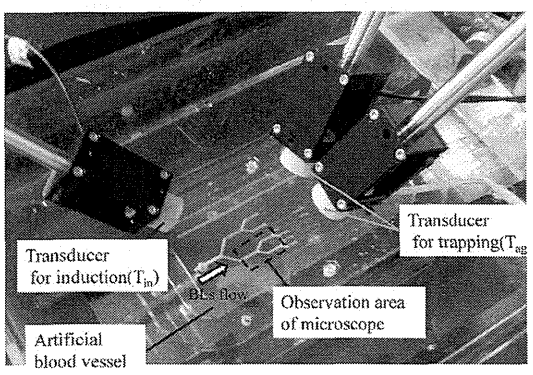

Fig. 4 Overview of the experimental setup with transducers and the artificial blood vessel.

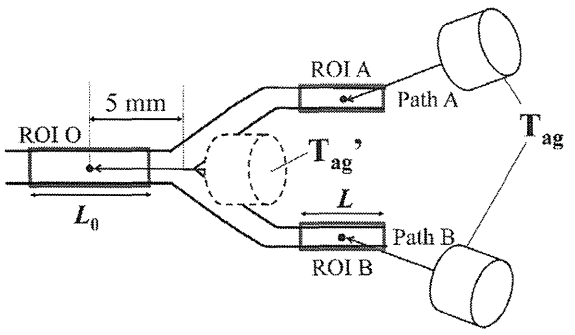

Fig. 5 Configuration between transducers T_{ag} and ROIs.

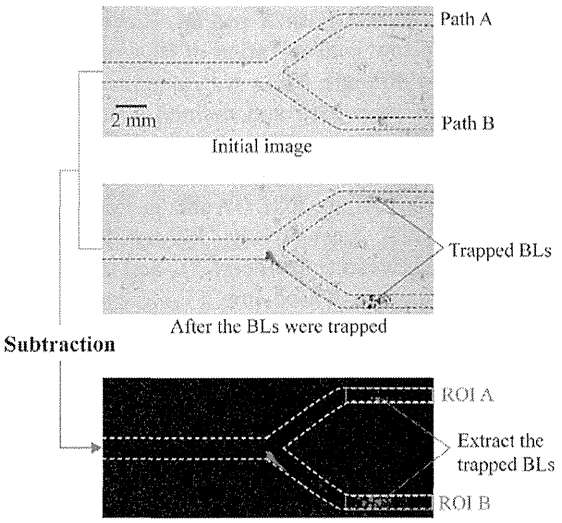

Fig. 6 Procedure to measure the area of trapped BLs in ROIs A and B.

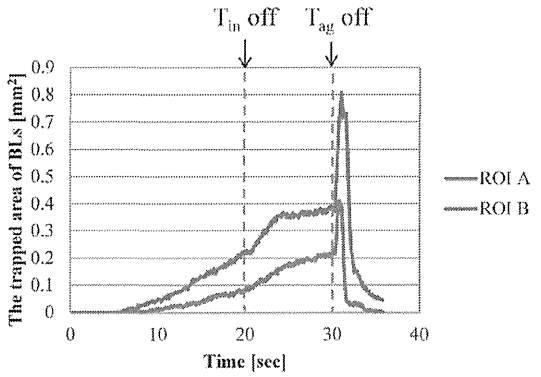

Fig. 7 Changes of the areas of trapped BLs in ROI A and ROI B over time.

zero. With the appearance of BLs, aggregates of BLs were trapped in both ROIs and the trapped areas increased simultaneously. A significant difference between the two ROIs was confirmed with T_{in} emission, indicating that larger amounts of BLs were propelled by T_{in} ultrasound emission. However, no significant difference between the two paths was observed without T_{in} emission (data not shown). A 3-ml aliquot of BL suspension was injected into the flow. The duration of injection was controlled by a rotary pump, set to finish approximately 20 s after the beginning of injection at a flow velocity of 40 mm/s. Then T_{in} emission was stopped at 20 s. Actually, all injected BLs were observed to have been delivered during 20–25 s. After 20 s, the trapped areas increased slightly, because the aggregates of BLs trapped at the bifurcation by T_{in} were removed and trapped at ROIs A and B. At 30 s, emissions by T_{ag} were stopped simultaneously, and thereafter the trapped area reached a maximum because the aggregates of BLs trapped by T_{ag} collapsed and apparently dispersed. At 30–40 s after the beginning of measurement, the trapped areas declined due to dis-

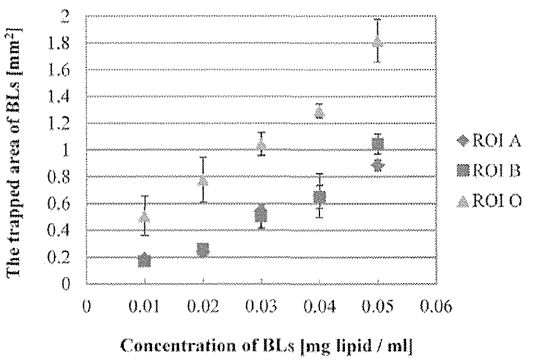

Fig. 8 The trapped area of BLs vs. concentration of BLs.

appearance of bubbles. Thus, we evaluated the area of trapped BLs at 20 s and 30 s, just before T_{in} and T_{ag} emissions were stopped, respectively. At 20 s and 30 s, we calculated the induction index ξ_B, which indicates that BLs are induced to Path B rather than Path A, using the following equation:

$$\xi_B = \frac{\sigma_B - \sigma_A}{\sigma_A + \sigma_B} \quad (1)$$

where σ_A and σ_B are the areas of trapped BLs in ROIs A and B, respectively.

Then, we confirmed the relationship between trapped area σ and concentration of BLs. To confirm the conservation of the number of BLs before and after the bifurcation, we measured the trapped areas in ROI O, ROI A and ROI B without ultrasound emission from T_{in}. Suspensions of BLs were prepared at five levels of concentrations ranging from 0.01–0.05 mg lipid/ml, and trapped in each ROI with the emission of T_{ag} and T_{ag}' as shown in **Fig. 5**. The areas of trapped BLs were measured for suspensions of various lipid concentrations with ultrasound emission at the maximum sound pressure of 500 kPa-pp. **Figure 8** shows the concentration of BLs vs the area of trapped BLs. The standard deviation of three trials is also shown in the figure. The trapped areas in ROI A and B were measured simultaneously, the trapped area of ROI O was measured independently.

As shown in **Fig. 8**, using BL concentrations of 0.01–0.05 mg lipid/ml, the area of BLs increased linearly as the concentration of BLs increased. The trapped area in ROI O was approximately two-fold larger than that in ROI A or B. We confirmed that the concentration of 0.02 mg lipid/ml, which was used in subsequent experiment, was within the range of linear change in trapped area.

3. Results

We observed BL behavior in the bifurcation upon emission of ultrasound from T_{in} and T_{ag}. **Figure 9** shows the serial extraction images of BLs in the observation area after the appearance of injected BLs with T_{in} emission at a frequency of 5 MHz, a flow velocity of 40 mm/s, and at a BL concentration of 0.02 mg lipid/ml. The outline of the blood vessel was overlapped as the white line in the top-left image. The bottom-left image is a close-up image of bifurcation area enclosed by the dotted line in the image

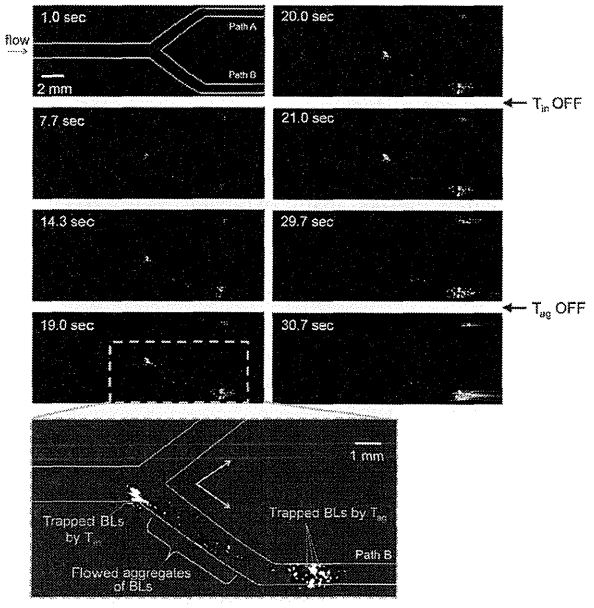

Fig. 9 Serial extraction images of BLs in the observation area.

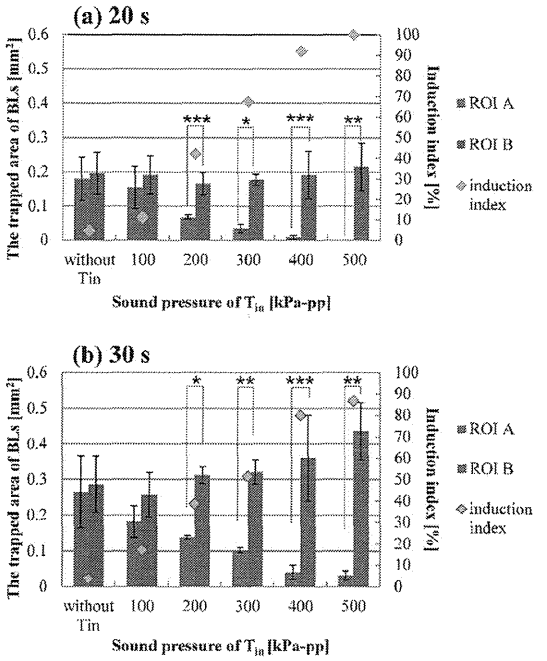

Fig. 10 The trapped area of BLs vs. sound pressure of T_{in} at 20 s (a), and at 30 s (b) with induction index. ($^{*}P < 0.01$, $^{**}P < 0.05$, $^{***}P < 0.1$).

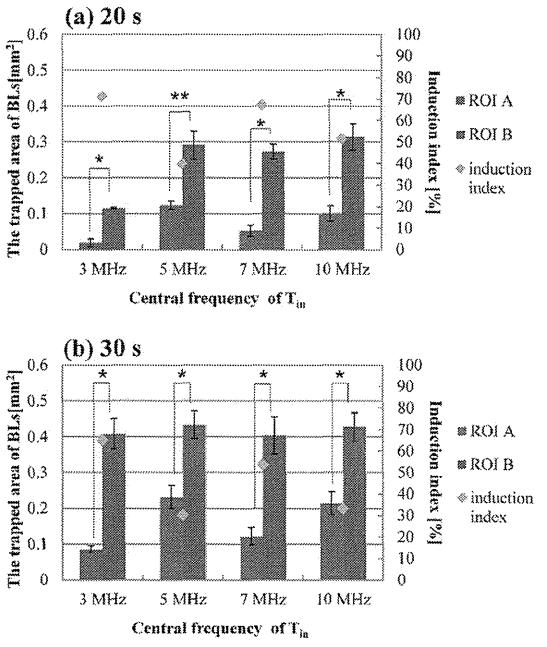

Fig. 11 The trapped area of BLs vs. central frequency of T_{in} at 20 s (a), and at 30 s (b) with induction index. ($^{*}P < 0.01$, $^{**}P < 0.05$).

of 19.0 s. We confirmed flowed aggregates of BLs in Path B after T_{in} emission although they were not observed before the emission. The aggregated BLs were trapped both in ROIs A and B. Up to 20 s, an increase in aggregation in ROI B was observed. On the other hand, an increase in area of BLs at the focal point of T_{in} in the bifurcation was also confirmed. When the ultrasound from T_{in} was stopped, most the BL aggregates trapped by T_{in} at the bifurcation collapsed and flowed into ROIs A and B. Most of the aggregates were trapped in the two ROIs in the duration from 20 s to 30 s, with additional increases in area of trapped BLs in both ROIs. After 30 s, the aggregates of BLs collapsed and disappeared.

We measured the areas of trapped BLs in ROIs A and B upon T_{in} emission at a frequency of 5 MHz, for a BL concentration of 0.02 mg lipid/ml, when the sound pressure was set at 100, 200, 300, 400 and 500 kPa-pp. **Figure 10** shows the areas of trapped BLs versus sound pressure of T_{in} at 20 s(a), and at 30 s(b). The standard deviation of three trials is also shown in the figure. Statistical significance was analyzed by *t*-test ($^{*}P < 0.01$, $^{**}P < 0.05$, $^{***}P < 0.1$). At 20 s, the area of trapped BLs in Path B (σ_B) remained unchanged at 0.2 mm^2 when the sound pressure was 300 kPa-pp or higher (**Fig. 10a**), because more BLs were trapped at the focal point of T_{in} at the bifurcation. At 30 s, the σ_B increased rapidly with an increase in sound pressure of T_{in} (**Fig. 10b**). Comparing **Fig. 10a and 10b**, the σ_B increased 1.35, 1.87, 1.81, 1.88 and 2.03 times at sound pressures of 100, 200, 300, 400 and 500 kPa-pp, respectively. When the sound pressure exceeded 300 kPa-pp, the induction indexes at 30 s were lower than those at 20s.

Next, we fixed the sound pressure at 200 kPa-pp, and repeated the same experiment with the central frequencies at 3, 5, 7 and 10 MHz. **Figure 11** shows the area of trapped BLs versus central frequency. The standard deviation of three trials is also shown in the figure. Statistical significance was analyzed by *t*-test ($^{*}P < 0.01$, $^{**}P < 0.05$). Comparing **Fig. 11a and 11b**, the σ_B increased 3.52, 1.49, 1.48 and 1.36 times at central frequency of 3, 5, 7 and 10 MHz, respectively. At 20 s,

especially at the frequency of 3 MHz, more BLs were trapped at the focal point of T_{in} in the bifurcation, with small trapped area in ROI B. Induction indexes at 30 s were all lower than those at 20s.

4. Discussion

From the result of **Fig. 9**, when the T_{ag} emission stopped, the aggregates of BLs in ROIs A and B collapsed. In our previous study [9], the aggregates of MBs Sonazoid maintained the shape even if after the ultrasound emission stopped, and therefore we can apply Sonazoid to a novel therapy, artificial embolization. This is a very different aspect between BLs and conventional MBs. In other words, there is no concern over embolization in ultrasound therapy using BLs. This difference seems to arise from the shell properties of BLs and Sonazoid. Sonazoid bubbles are bound to each other because of surface interaction of the lipid membrane without PEG modification, resulting in long-lasting bonding with each other.

BLs with average diameters of 400 to 500 nm should be subjected to 16 to 25 times less force than MBs that had an average diameter of 2 μm, because the primary Bjerknes force [7, 8] is proportional to the cross-sectional area of the objects. However, we succeeded to trap BLs at the same range of sound pressure as for MBs in this experiment. It was probably the effect of aggregation caused by secondary Bjerknes force under ultrasound emission. Because of the increased cross-sectional area caused by aggregation, the aggregates of BLs would be propelled easily. In terms of trapping efficiency, we have to consider not only the differences in diameter and shell properties, but also aggregate formation and interaction between surface of bubbles and vessel walls.

The induction index was proportional to sound pressure (**Fig. 10**). This tendency was consistent with MBs [6, 7]. Further study is required to clarify the sound pressure level for destruction of BLs. Under the threshold of sound pressure for shell destruction, BLs may be used as a carrier for gene and drug delivery until they arrive at their final destination inside the body. Furthermore, the threshold is very important for drug release.

More BLs were trapped on the vessel wall at the bifurcation point by exposure to T_{in}, especially at the frequency of 3 MHz (**Fig. 11**). This occurred probably because of the wider beam width of ultrasound. The overlapped area of ultrasound beam on the vessel wall becomes larger as frequency becomes lower. Furthermore, the size of aggregates increases at lower frequencies [13], apparently increasing the amount of trapped BLs. To avoid trapping BLs at the bifurcation, thinner beam width and higher frequency are required.

In the next step, we will elucidate the behavior of BLs in a viscous flow before applying it to an *in vivo* experiment. The effect of hematocrit of human blood should be considered to determine the viscosity of fluid medium. We will also develop a method of identifying fluorochrome-labeled BLs *in vivo*.

5. Conclusions

In this study, we achieved active control of BLs with diameters of 400 to 500 nm, orientating these BLs to flow into the desired path of a bifurcated blood vessel. To measure the controllability of BLs quantitatively, we designed a new method using two transducers to evaluate the areas of trapped BLs in the two paths after the bifurcation, to determine which path has increased BLs. We investigated the ultrasound conditions for active path selection of BLs, in terms of the sound pressure and frequency. We found that more BLs can be oriented to a desired path at higher sound pressure. To avoid trapping BLs at the bifurcation, higher frequency is required. For further analysis, we are aiming at active control of BLs *in vivo*.

Acknowledgement

This research was supported by the Japan Society for the Promotion of Science (JSPS) through the Funding Program for Next Generation World-Leading Researchers (NEXT Program).

References

1. Kajiyama K, Yoshinaka K, Takagi S, Matsumoto Y: Microbubble enhanced HIFU. Phys Procedia. **3**(1), pp. 305-314, 2010.
2. Chung DJ, Cho SH, Lee JM, Hahn ST: Effect of microbubble contrast agent during high intensity focused ultrasound ablation on rabbit liver *in vivo*. Eur J Radiol. **81**(4), e519-e523, 2012.
3. Sasaki N, Kudo N, Nakamura K, Lim SY, Murakami M, Kumara WR, Tamura Y, Ohta H, Yamasaki M, Takiguchi M: Activation of microbubbles by short-pulsed ultrasound enhances the cytotoxic effect of cis-diamminedichloroplatinum (II) in a canine thyroid adenocarcinoma cell line *in vitro*. Ultrasound Med Biol. **38**(1), pp. 109-118, 2012.
4. Osawa K, Okubo Y, Nakao K, Koyama N, Bessyo K: Osteoinduction by microbubble-enhanced transcutaneous sonoporation of human bone morphogenetic protein-2. J Gene Med. **11**(7), pp. 633-641, 2009.
5. Juffermans LJM, van Dijk A, Jongenelen CAM, Drukarch B, Reijerkerk A, de Vries HE, Kamp O, Musters RJP: Ultrasound and microbubble-induced intra-and intercellular bioeffects in primary endothelial cells. Ultrasound Med Biol. **35**(11), pp. 1917-1927, 2009.
6. Masuda K, Muramatsu Y, Ueda S, Nakamoto R, Nakayashiki Y, Ishihara K: Active path selection of fluid microcapsules in artificial blood vessel by acoustic radiation force. Jpn J Appl Phys. **48**(7), 07GK03, 2009.
7. Masuda K, Watarai N, Nakamoto R, Muramatsu Y: Production of local acoustic radiation force to constrain direction of microcapsules in flow. Jpn J Appl Phys. **49**, 07HF11, 2010.
8. Masuda K, Nakamoto R, Watarai N, Koda R, Taguchi Y, Kozuka T, Miyamoto Y, Kakimoto T, Enosawa S, Chiba T: Effect of existence of red blood cell in trapping performance of microbubbles by acoustic radiation force. Jpn J Appl Phys. **50**, 07HF11, 2011.
9. Shigehara N, Demachi F, Koda R, Mochizuki T, Masuda K:

Experimental study of active path block in a multi-bifurcated flow by microbubble aggregation. J Appl Phys. **52**, 07HF15, 2013.
10. Suzuki R, Takizawa T, Negishi Y, Utoguchi N, Maruyama K: Effective gene delivery with novel liposomal bubbles and ultrasonic destruction technology. Int J Pharm. **354**, pp. 49–55, 2008.
11. Koda R, Koido J, Ito T, Mochizuki T, Masuda K, Ikeda S, Arai F, Miyamoto Y, Chiba T: Experimental study to produce multiple focal points of acoustic field for active path selection of microbubbles through multi-bifurcation. Jpn J Appl Phys. **52**, 07HF13, 2013.
12. Kudo N, Sakaguchi K, Suzuki R, Maruyama K: Effects of phase transition of a lipid bilayer on dynamics of Bubble liposomes. Proc of IEEE Ultrasonics Symposium 2009. IEEE, Rome, 2009, pp. 1255–1258.
13. Koda R, Watarai N, Shigehara N, Ito T, Minamide A, Masuda K, Kakimoto T, Enosawa S, Miyamoto Y, Chiba T: Study of aggregate formation of microbubbles under ultrasound exposure and effect with red blood cells. Trans Jpn Soc Med Biol Eng. **50**, pp. 138–148, 2012[in Japanese].

Ren KODA

Ren KODA received the B.Eng. and M.Eng. degrees from Chiba University, Japan in 2009 and in 2011, respectively and the Ph.D. degree in Engineering from Tokyo University of Agriculture and Technology, Japan in 2014. He is currently a Research Assistant Professor of Science and Engineering for Research at University of Toyama, Japan. His research interests include ultrasonic therapy using microbubbles and non-destructive inspection using ultrasound.

Jun KOIDO

Jun KOIDO received the B.E. degree in Engineering from Tokyo University of Agriculture and Technology, Japan in 2013. His research interest is microbubble delivery using ultrasound in blood vessel for his master degree.

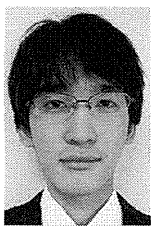

Naoto HOSAKA

Naoto HOSAKA received the B.Eng. and M.Eng. degrees from Tokyo University of Agriculture and Technology, Japan in 2013 and in 2014, respectively. He is currently a Doctorial course student, Tokyo University of Agriculture and Technology, Japan. His research interest is microbubble manipulation in blood vessel for therapy.

Shinya ONOGI

Shinya ONOGI received the B.Eng. and M.Eng. degrees from Hokkaido University, Japan in 2002 and in 2004, respectively, and the Ph.D. degree in Science from the University of Tokyo, Japan in 2007. From 2007 to 2009, he was a Project Researcher of Intelligent Modeling Laboratory at the University of Tokyo. From 2009 to 2010, he was a Postdoctoral Fellow of Mechanical Engineering at Johns Hopkins University, USA. He is currently a Specially Appointed Assistant Professor (NEXT Program, JSPS) of Bio-Applications and Systems Engineering at Tokyo University of Agriculture and Technology, Japan. His research interests are computer assisted surgery/therapy based on robotics and information science.

Takashi MOCHIZUKI

Takashi MOCHIZUKI received the B.Eng. and Ph.D. degrees from Tokyo University of Agriculture and Technology, Japan, in 1976 and 1994, respectively. From 1976 to 2012, he worked for Hitachi Aloka Medical, Ltd. After the company retirement, he established a startup company to consult the ultrasound technology and has become CEO. Also, he has been a Specially Appointed Professor (NEXT Program, JSPS) of Graduate School of Bio-Applications and Systems Engineering, Tokyo University of Agriculture and Technology. His research interests include therapeutic applications in ultrasound and bioeffects of ultrasound.

Kohji MASUDA

Kohji MASUDA received the B.Eng., the M.Eng. and Ph.D. degrees from Osaka University, Japan, in 1991, 1993, and 1996, respectively. From 1996 to 1999, he was an Assistant Professor with Nagoya University, Japan. From 1999 to 2002, he was an Assistant Professor with Ehime University, Japan. From 2002 to 2003, he was an Postdoctoral Fellow with Universite Grenoble I-Joseph Fourier, France. Since 2003, he has been an Associate Professor with Graduate School of Bio-Applications and Systems Engineering, Tokyo University of Agriculture and Technology, Japan. His research interests include therapeutic applications in ultrasound, medical robotics, and medical image processing.

Ryo SUZUKI

Ryo SUZUKI graduated the school of pharmacy, Tokyo university of Pharmacy and Life Sciences, Japan in 1996 and received Ph.D. (Pharmaceutical Sciences) from Graduate School of Pharmaceutical Sciences, Osaka University, Japan in 2001. He is currently an associated professor, School of Pharma-Sciences, Teikyo University, Japan. His research interest is drug and gene delivery system with liposome and ultrasound.

Kazuo MARUYAMA

Kazuo Maruyama graduated School pharmacy, Tokyo University of Pharmacy and life Science, Japan in 1977 and received Master's (Pharmacy) degree from Graduate school of Kumamoto University, Japan, in 1979. He received Ph.D. degrees from Tokyo University of Pharmacy and life Science, Japan, in 1986. He was an Assistant Professor and an Associate Professor with School of Pharmacy, Teikyo University from 1977 to 1988, and from 1994 to 2002, respectively. From 1988 to 1990, he was a Postdoctoral Fellow with University of Tennessee, USA. Since 2002 he has been a Professor with School of Pharmacy, Teikyo University, Japan. His research interests include liposomal drug deliver system, and theranostics which can diagnosis and therapy in combination of nanobubble and ultrasound.